ADVANCES IN ATMOSPHERIC SCIENCES, VOL. 23, NO. 1, 2006, 23–32

Temporal Structures of the North Atlantic Oscillation and Its Impact on the Regional Climate Variability

HUANG Jianping*[1] (黄建平), JI Mingxia[1] (季明霞), Kaz HIGUCHI[2], and Amir SHABBAR[2]

[1]*College of Atmospheric Sciences, Lanzhou University, Lanzhou* 730000

[2]*Meteorological Service of Canada*, 4905 *Dufferin Street, Downsview, Ontario, Canada* M3H 5T4

(Received 31 January 2005; revised 25 July 2005)

ABSTRACT

In this study, the temporal structure of the variation of North Atlantic Oscillation (NAO) and its impact on regional climate variability are analyzed using various datasets. The results show that blocking formations in the Atlantic region are sensitive to the phase of the NAO. Sixty-seven percent more winter blocking days are observed during the negative phase compared to the positive phase of the NAO. The average length of blocking during the negative phase is about 11 days, which is nearly twice as long as the 6-day length observed during the positive phase of the NAO. The NAO-related differences in blocking frequency and persistence are associated with changes in the distribution of the surface air temperature anomaly, which, to a large extent, is determined by the phase of the NAO. The distribution of regional cloud amount is also sensitive to the phase of the NAO. For the negative phase, the cloud amounts are significant, positive anomalies in the convective zone in the Tropics and much less cloudiness in the mid latitudes. But for the positive phase of the NAO, the cloud amount is much higher in the mid-latitude storm track region. In the whole Atlantic region, the cloud amount shows a decrease with the increase of surface air temperature. These results suggest that there may be a negative feedback between the cloud amount and the surface air temperature in the Atlantic region.

Key words: North Atlantic Oscillation, atmospheric blocking, cloud, negative feedback

1. Introduction

The North Atlantic Oscillation (NAO) is a dominant mode of atmospheric variability in the North Atlantic sector, accounting for more than 30% of the hemispheric variability in the surface pressure data (Cayan, 1992). Although the NAO pattern is most pronounced during the winter season, it is identifiable throughout the year. The NAO has been used to describe climatic variability in such parameters as temperature and precipitation over regions extending from eastern North America to western and central Europe (Walker and Bliss, 1932; van Loon and Rogers, 1978; Barnston and Livezey, 1987; Hurrell, 1995; Li and Wang, 2003). Applying complex empirical orthogonal function analysis to gridded sea level pressure fields obtained from observation and simulation runs from two GCMs (one from the Geophysical Fluid Dynamic Laboratory and the other from the National Center for Atmospheric Research), Barnett (1985) demonstrated that the NAO is a "natural mode of spatial response (standing wave) of the global climate system", and is generated by the nonlinear internal dynamics of the atmospheric circulation alone. The NAO is characterized by variations on multiple timescales. For example, Hurrell and van Loon (1997) showed a power spectrum of the NAO index for the 130 winters from 1865 to 1994, revealing significant variance in the quasibiennial periods, as well as enhanced power in the 6- to 10-year period band. They stated that the latter period band "has become more pronounced over the latter half of this century". Rogers (1984), Cook et al. (1998), and Schneider and Schonwiese (1989) also found multiple spectral peaks at various timescales.

The NAO is to a great extent responsible for determining the surface thermal configuration in the North Atlantic, in eastern North America and in the Eurasian sector (Nesterov, 1998; van Loon and Rogers, 1978). Changes in the phase of the NAO are associated with basin-wide changes in the intensity and location of the North Atlantic jet stream and storm track. The NAO also modulates large-scale patterns of zonal

*E-mail: hjp@lzu.edu.cn

and meridional heat and moisture transport (Hurrell, 1995), which in turn results in changes in temperature and precipitation patterns which often extend from eastern North America to western and central Europe (Walker and Bliss, 1932; van Loon and Rogers, 1978). The interannual to interdecadal changes in the frequency of blocking formations in the North Atlantic may also be related to the changes in the surface thermal forcing induced by different phases of the NAO (Shabbar et al., 2001). In order to give some insight into the possible mechanism for the regional climate variability, a systematic examination of the relationship between the NAO and blocking as well as that between the NAO and cloud will be undertaken in this study.

In sections 2 and 3, the multiresolution spectral analysis and the dataset used in this study are described, respectively. The impact of the NAO on circulation anomalies is presented in section 4. The impacts of the NAO on blocking and cloud are discussed in sections 5 and 6, respectively. The conclusions and discussion are given in section 7.

2. Multiresolution spectral analysis

In this section, we briefly review some relevant aspects of the multiresolution spectral and cross-spectral analysis used in this study. The method combines the windowed Fourier transform and the wavelet transform into a single transform which has some specific advantages for studying geophysical signals. Further details regarding this technique can be found in Wilson et al. (1992), Stockwell et al. (1996) and Huang et al. (1997). A very useful introduction to the application of wavelet analysis to meteorological data is given by Torrence and Compo (1998). For detailed discussions of the wavelet analysis of time series, the reader is encouraged to refer to these published articles, as well as the references therein. We will give only a very brief description here.

For a continuous one-dimensional time series $x(t)$, its continuous multiresolution Fourier transform at time τ, frequency f, and scale σ is defined by

$$F_{\rm m}(f,\tau,\sigma) = \int_{-\infty}^{+\infty} x(t) g(t-\tau,\sigma) e^{-i2\pi f t} dt \,, \qquad (1)$$

where $g(t,\sigma)$ is an appropriate window function. The dilation, or scaling, parameter σ increases the "width" of the window function for lower frequencies, while decreasing if for higher frequencies; it is controlled by selecting a specific functional dependence of σ with frequency f. Following Huang et al. (1997), we use the Gaussian window as the window function, and choose $\sigma = 1/f$.

In essence, this transform takes a one-dimensional function of time and changes it into a two-dimensional function of time and frequency. For a given scale parameter σ as a function of f, we write $F_{\rm m}(f,\tau,\sigma)$ as $F_{\rm m}(f,\tau)$, which is a complex function with amplitude and phase defined by

$$A(f,\tau) = |F_{\rm m}(f,\tau)| \qquad (2)$$

and

$$\Phi(f,\tau) = \arctan \frac{{\rm Im}[F_{\rm m}(f,\tau)]}{{\rm Re}[F_{\rm m}(f,\tau)]} \,, \qquad (3)$$

respectively. From the amplitude and phase defined above, we obtain a sinusoidal function,

$$C(f,\tau) = A(f,\tau)\cos[2\pi f t + \Phi(f,\tau)] \,, \qquad (4)$$

which provides a combined depiction of amplitude and phase at a given frequency. The function $C(f,\tau)$, evaluated at a particular frequency f, is called the "component".

Following a direct analogy with Fourier power spectra, we can readily define the multiresolution spectral density as

$$S_{\rm m}(f,\tau) = F_{\rm m}(f,\tau) F_{\rm m}^{*}(f,\tau) = |F_{\rm m}(f,\tau)|^2 \,, \qquad (5)$$

where $()^*$ indicates the complex conjugate of ( ).

Essentially, all the fundamental results of the theory of multiresolution spectral analysis are generalizations of the results from the conventional theory of Fourier spectral analysis, in the sense that the latter is the average value of the former for which the time series is purely stationary. The statistical significance test procedure used in this study was developed by Torrence and Compo (1998). The procedure is based on comparing theoretical wavelet spectra for white and red noise with Monte Carlo results. These spectra are then used to establish null hypothesis significance tests.

3. Data

In this study, we use the 138-year time series of the monthly NAO index from January 1865 through March 2003. The first NAO index was defined by Walker and Bliss (1932) and subsequently simplified by Rogers (1984), who constructed an NAO index starting in 1894, using sea level pressure (SLP) anomalies from Ponta Delgados, Azores and Akuyreyri, Iceland. Hurrell (1995) selected Lisbon, Portugal and Stykkisholmur, Iceland in order to extend the record back another 30 years; the time series of this index is the one employed here. Because an NAO index based on station pressure is affected by small-scale and transient meteorological phenomena unrelated to NAO, the index is smoothed using a 7-point low-pass running mean filter to remove fluctuations with periods roughly less than six months. In the present study, this smoothed data constitute our NAO index data base. The 500-hPa height and surface air temperature dataset used in this study is composed of the

daily and monthly averaged NCEP re-analysis data (Kalnay et al., 1996) from January 1948 to February 2004 and the spatial resolution of the data is 2.5° by 2.5°. An objective blocking index from 1958 to December 1996 as defined by Tibaldi and Molteni (1990) is used throughout this study. The nature of the blocking index and the criteria used in its construction are extensively discussed in Tibaldi and Molteni (1990). The cloud data used in this study are the ISCCP (International Satellite Cloud Climatology Project) D2 monthly mean data from July 1983 to September 2001 and the spatial resolution of the data is 2.5° by 2.5°. The ISCCP was established in 1982 as part of the World Climate Research Programme (WCRP) to collect and analyze satellite radiance measurements to infer the global distribution of clouds, their properties, and their diurnal, seasonal, and interannual variations.

Throughout our study, each winter, from 1948–49 through 2002–03, is defined as the period beginning on 1 December and ending on 31 March of the following year; and the value for year N refers to the average of December in year $N-1$ and January, February, and March in year N (DJFM).

4. The impact of NAO

4.1 *The impact on circulation anomalies*

Figure 1 shows the anomaly variation and its linear trend for the NAO index. The NAO index shows a marked upward long-term trend, consistent with previous studies (e.g., Hurrell, 1995, 1996). Figure 2 shows a multiresolution spectrum of the NAO index in the period and time domain. It should be noted that the spectrum is normalized by N/σ^2, where N is the number of data points and σ^2 is the variance of the time series. Under this normalization, white noise has an expectation value of 1 at all frequencies (Torrence and Compo, 1998). The thick contours enclose regions of

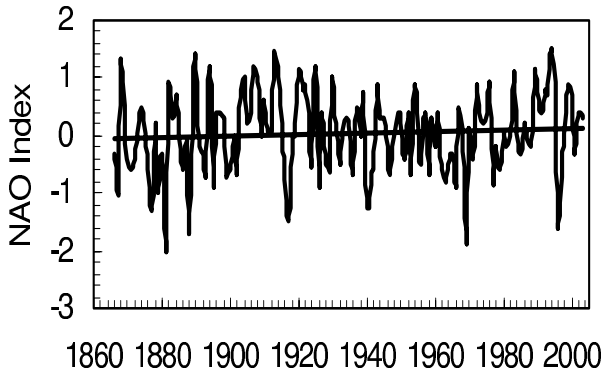

Fig. 1. Anomaly variation and its long-term trend for the NAO index.

statistical significance greater than 95%; the statistical significance test procedure used here is the one developed by Torrence and Compo (1998). The most noticeable feature in the period-time spectrum in Fig. 2 is that the temporal spectral structure of the NAO is characterized by three period bands: (1) annual cycle (1–2 years), (2) interannual cycle (2–10 years), and (3) decadal cycle (>10 years). The modulation of the NAO is strongly influenced by the presence of the interannual component prior to 1900, with an exception around 1880 when most of the spectral terms ranging from annual to decadal appear to have contributed to the overall NAO variation. The interannual contribution is relatively weak from around 1890 to 1910. From around 1910 to about 1925, there is a gradual shift in the contribution from higher periodic terms of the interannual component to the decadal component, although just prior to 1920, there is evidence of a simultaneous contribution by periodicities ranging continuously from about 4 years to decades. On the annual timescale, the multiresolution spectrum visibly

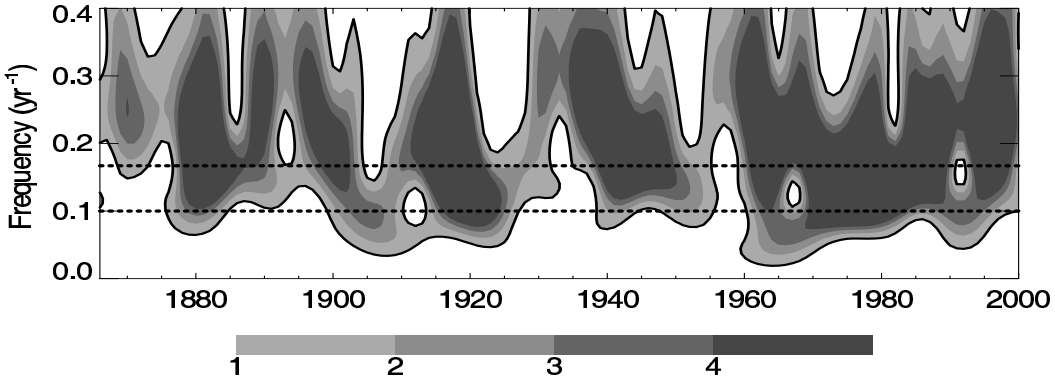

Fig. 2. Multiresolution spectrum of the NAO index time series. The solid black lines enclose those regions with statistical significance greater than the 95% level. 6-and 10-year period components are identified by the horizontal dashed lines.

Table 1. Years in which the NAO remained in the top tenth percentile (negative) and the bottom tenth percentile (positive) for the December-to-March period. These years are chosen to study the behaviour of the 500-hPa height and surface air temperature in the North Atlantic. Years are labelled on January of the averaging period.

Negative NAO	1955	1962	1963	1964	1965	1966	1969	1977	1979	1996
Positive NAO	1961	1973	1983	1989	1990	1993	1994	1995	1999	2000

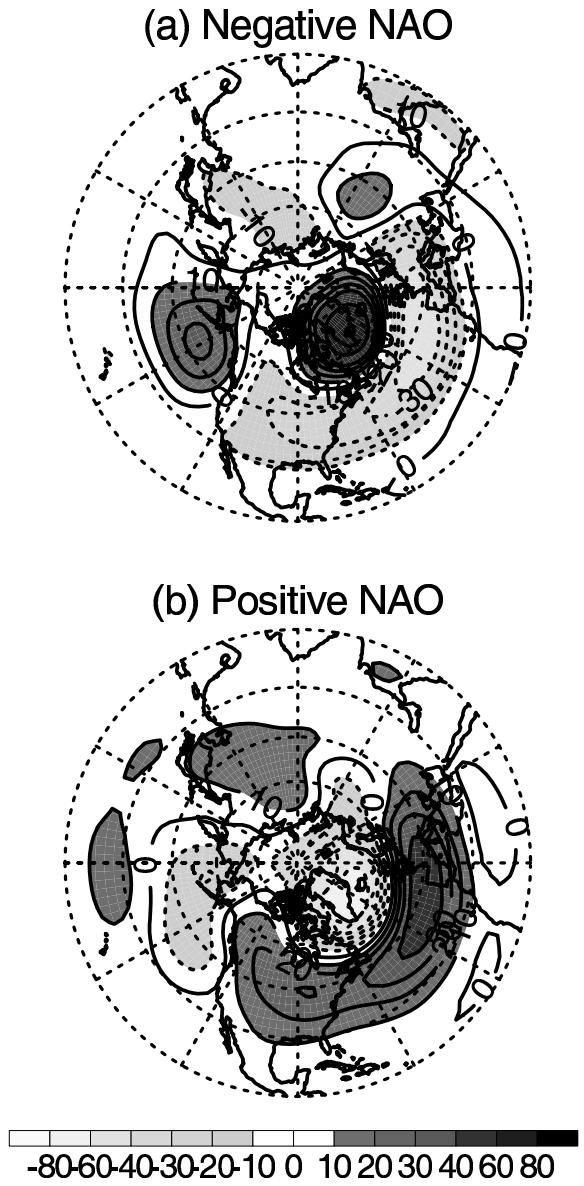

Fig. 3. Composite 500-hPa height anomaly field, in decameters (dam), of the winter (December through March) associated with (a) negative NAO and (b) positive NAO.

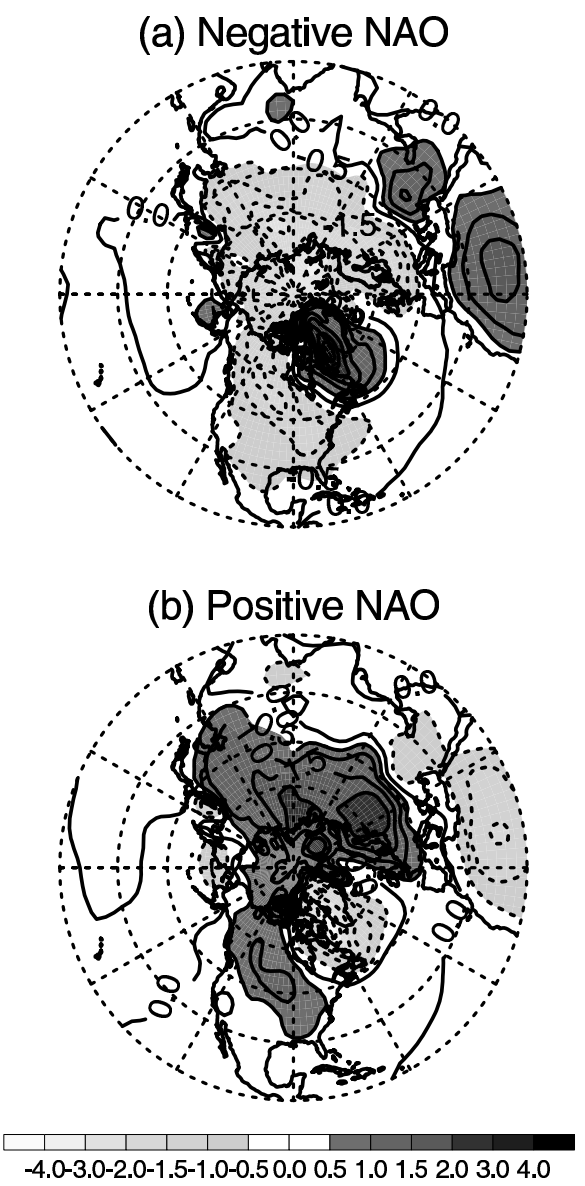

Fig. 4. Composite surface air temperature (°C) anomaly field of winter (December through March) associated with (a) negative NAO and (b) positive NAO.

discloses fluctuations in both the amplitude and frequency of the annual cycle. The recognizable presence of the spectral signature around the annual timescale implies that the interaction between the NAO and the annual cycle is very important. On the interannual timescale, most of the power is concentrated within the period band of 2–10 years.

Changes in the NAO indices are often accompanied

Table 2. Correlation coefficients between monthly NAO and regional blocking index in the period of December to March.

Region	Pacific 170°E–130°W	Canada 130°–60°W	Atlantic 60°W–10°E	Europe 10°–80°E	Siberia 80°–170°E
Correlation	0.08	−0.45	−0.54	0.017	−0.09

Table 3. Years in which the NAO remained in the top tenth percentile (negative) and the bottom tenth percentile (positive) for the December-to-March period. These years are chosen to study the behaviour of blocking in the North Atlantic. Years are labelled on January of the averaging period.

Negative NAO	1962	1963	1964	1965	1966	1969	1970	1977	1979	1996
Positive NAO	1973	1975	1981	1983	1989	1990	1992	1993	1994	1995

by changes in the atmospheric circulation patterns over the Northern Hemisphere. In order to explore the effect of NAO on the circulation anomalies, we compare the composite winter (DJFM, following Hurrell, 1995) 500-hPa height anomalies associated with the years of negative and positive phases of NAO as shown in Fig. 3. For both phases, a set of 10 years (see Table 1) are chosen to construct a composite 500-hPa winter anomaly field shown in Fig. 3. For the negative phase of NAO, the dominant winter 500-hPa atmospheric circulation anomaly field is shown in Fig. 3a. Negative and positive anomalies over the western and eastern North Pacific, respectively, are present. A large zonal band of strong negative anomaly stretches from the U. S.–southern Canada, across the Atlantic Ocean to western Europe, and is bordered on the north by an area of predominantly positive anomaly located over northern Canada and Greenland. The dominant 500-hPa teleconnection pattern associated with the positive phase, shown in Fig. 3b, has a positive anomaly center over the tropical North Pacific, a negative anomaly over the northern North Pacific, followed by a positive anomaly over most of Canada. A negative anomaly center is located over the southern U.S. and Mexico. Also evident is a positive anomaly center over the North Atlantic west of Europe.

Figure 4 compares the composite wintertime surface air temperature anomalies (SATA) associated with the two phases of the NAO. For the negative phase of NAO, the distribution of the SATA shows a general but distinctive "warm ocean/cold land" pattern across the mid and high latitudes of the North Atlantic basin (Fig. 4a). The warming is centered over Baffin Bay/Labrador Sea and the western North Atlantic. In this case, where the surface thermal forcing pattern is associated with the negative NAO, the zonally-asymmetric thermal forcing and topographic forcing are basically in phase, i.e., heating over ocean and the cooling over land. For the positive phase of the NAO, the distribution of the SATA anomalies reflects the "cold ocean/warm land" pattern (Fig. 4b). In this case, the zonally-asymmetric thermal and topographic forcings are out of phase, i.e., cooling over ocean and heating over land.

4.2 *The impact on blocking*

Figure 5 shows the anomaly variation and its linear trend for the the Atlantic blocking index. The Atlantic blocking index shows a systematic downward trend during the past 39 years. Note the marked change toward the negative phase of the NAO (see Fig. 1) and the attendant rise in blocking days in the mid 1990s. To examine the linear relationship between the NAO and the regional blocking activity, correlation coefficients between the monthly NAO and the regional blocking index for the December-to-March period are calculated (Table 2). The correlation coefficients are based on a sample size of 38×4=152 values (38 years and 4 months per year). The correlation coefficient between the NAO and the blocking index is −0.45 for the Canadian region and −0.54 for the North Atlantic region, with both correlation values being statistically significant at the 99% level of significance; there is no significant response in any of the other regions. This suggests that the effect of the different phases of the NAO on blocking is localised to the North Atlantic and the Canadian regions. The frequency of blocking events in these two regions tends to be higher during the winter in which the NAO is in the negative phase.

Blocking days are quantified in Fig. 6 with respect to the negative (white) and the positive (black) phases of the NAO. The composite years for the negative and positive NAO are listed in Table 3. The frequency of wintertime blocking in the North Atlantic region is approximately 67% greater during the negative phase of the NAO than during the positive phase. During the negative phase, the average number of blocking days in the Atlantic region is 52.8, which is statistically different from the climate mean of 31.7 days at the 95% level. For the positive phase of the NAO index, the average number of blocking days is 19.4, again statistically different from the climatic mean. The difference

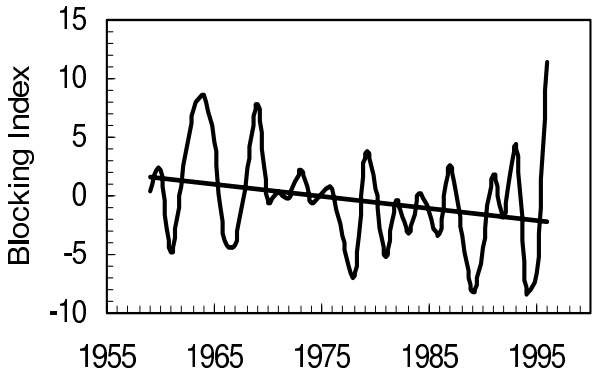

Fig. 5. Anomaly variation and its long-term trend for the blocking index over the northern Atlantic region.

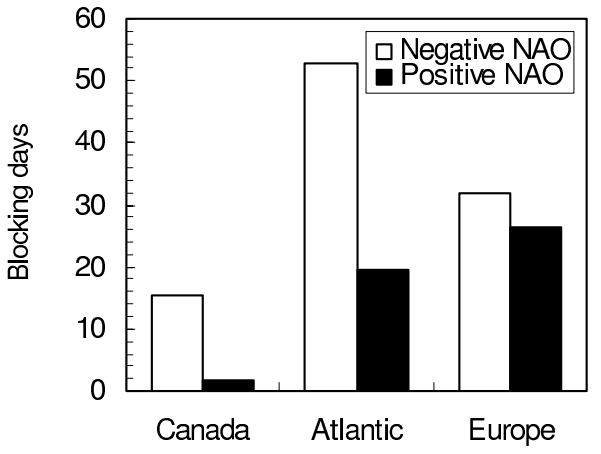

Fig. 6. Composite days of regional blocking events for (a) negative NAO (white) and (b) positive NAO (black). The difference between the two phases of the NAO is significant at the 95% level for the Canadian and the Atlantic regions.

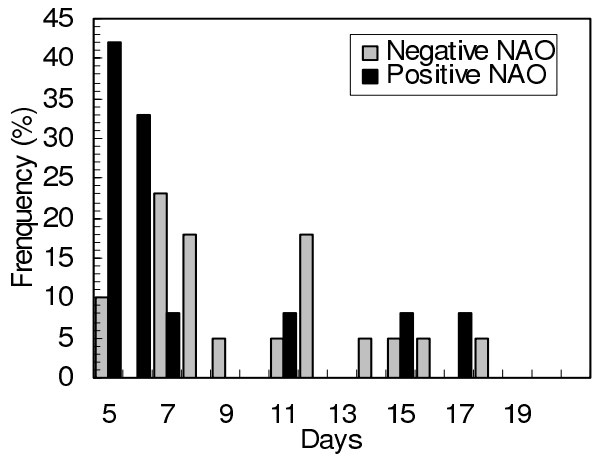

Fig. 7. Frequency distribution of blocking duration longer than five days in the Atlantic region for (a) negative NAO (grey) and (b) positive NAO (black).

in blocking days from the climatic mean is also significant during the two phases of the NAO for the Canadian region. Results are similar if the composite period is changed to the months of January through March, or January through February. Since the blocking events in the Canadian region are much fewer than in the North Atlantic region, we will focus our attention on the relationship between the NAO and the North Atlantic blocking.

The frequency distribution of blocking duration for the two phases of the NAO are shown in Fig. 7, suggesting a strong dependency on the phasing of the NAO. When the NAO is in the positive phase, the duration of blocking is mainly in the 5-to-6-day range, with more than 70% of the blocking lasting less than 6 days. In contrast, during the negative phase of the NAO, only 5% of the blocking lasts less than 6 days, and the distribution of blocking duration covers a wide range from 5 to 18 days. The average duration is around 11 days, which is much longer than the duration associated with the positive phase of the NAO (about 6 days). Dole (1989) showed that the development and decay of persistent anomalies in the North Atlantic occur rather rapidly with a de-correlation time of about 10 days.

Although there is not a generally accepted theory for the dynamics of blocking, it has been recognised that nonlinear interaction and surface thermal forcing are the two essential factors (Charney and DeVore, 1979). Since topography is time invariant, the inter annual variability of the surface thermal forcing should be related to the inter annual variation of blocking. For the negative phase of the NAO, the zonally-asymmetric thermal forcing and topographic forcing are basically in phase, i.e., heating over ocean and cooling over land (see Fig. 4a). The thermal forcing acts in concert with the resonance forcing of the topography, and in accordance with Charney and DeVore's low-order model (Charney and DeVore, 1979), produces an environment favourable for the formation and persistence of blocking. For the positive phase of the NAO, however, the distribution of the SATA anomalies reflects the "cold ocean/warm land" pattern (see Fig. 4b) and the zonally asymmetric thermal and topographic forcings are out-of-phase, i.e., cooling over ocean and heating over land. The thermal forcing reduces or destroys the resonance forcing of the topography, making block formation difficult, though not impossible (Shabbar et al., 2001).

4.3 *The impact on cloud*

Cloud amount is higher in the mid-latitude storm tracks and in the convective zone in the Tropics. The regional cloud amount variations at low and middle latitudes are much larger than at higher latitudes, but there is usually less cloud amount over land than

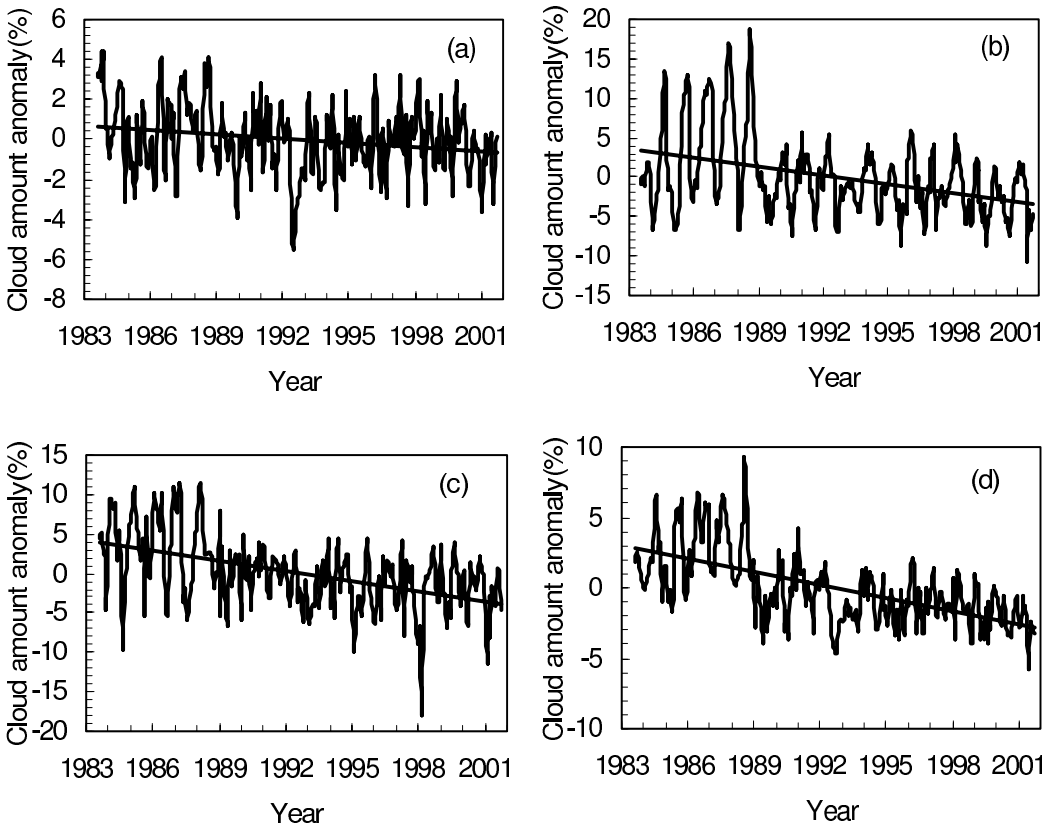

Fig. 8. Anomaly variation and its long-term trend for the regionally averaged cloud amount. (a) high latitudes (50°–70°N, 60°W–10°E) (b) mid latitude (20°–50°N, 60°W–10°E) (c) low latitude (0°–20°N, 60°W–10°E) and (d) total Atlantic region (0°–70°N, , 60°W–10°E).

ocean. Figure 8 shows the month-to-month variations for the Atlantic regionally-averaged cloud amount. The cloud amounts vary by about 2%–4% in the high-latitude (50°–70°N, 60°W–10°E) region, 5%–20% in the mid-latitude (20°–50°N, 60°W–10°E) region, and 5%–10% in the low-latitude (0°–20°N, 60°W–10°E) region. The short ISCCP historical record, covering only about 20 years, shows some signs of a slower variation. The cloud amount shows a decreasing trend from 1983 to 2001 in all the regions. Since a number of events occurred during this time period, the cause of these cloud variations is not yet understood.

Figure 9 shows how the scatter plot of cloud amount varies with surface temperature. Consistent with some previous studies (Lindzen et al., 2001; Ding et al., 2004), the cloud amount decreases with increases in the surface air temperature in all the regions. These results suggest that there may be a negative feedback between the cloud amount and the surface air temperature. As the surface temperature increases, so the rate of evaporation from the (warmer) oceans increases, supplying the atmosphere with more water vapour conducive to enhanced cloud formation. With greater cloud coverage, more incident radiation is reflected, reducing radiative forcing and leading to a lowering of the surface temperature. Lindzen et al. (2001) recently reported that the ratio between cloud amounts over the tropical western Pacific oceanic area (30°N–30°S, 130°E–170°W) has a negative correlation with sea surface temperature (SST). Based on this observation, along with an estimate of the mean radiative properties of these clouds, they examined a simple radiative energy balance model (3.5-box greenhouse model) to infer that these tropical clouds could provide a strong negative climate feedback for greenhouse-gas-induced global warming (-0.45 to about $-1.1\,\mathrm{K\,K^{-1}}$). According to Lindzen et al. (2001), decreases in cloud amount with increased surface temperature would allow more thermal longwave radiation to emit into space and, therefore, would cool the climate system. This feedback would be sufficiently strong enough to potentially negate many of the positive feedbacks—such as atmospheric water vapor—found in current climate models (e.g., Del Genio et al., 1991). Using ISCCP D2 data, Ding et al. (2004) also found that global warming in the past 20 years has made the cloud amount decrease, and the decrease of the cloud amount

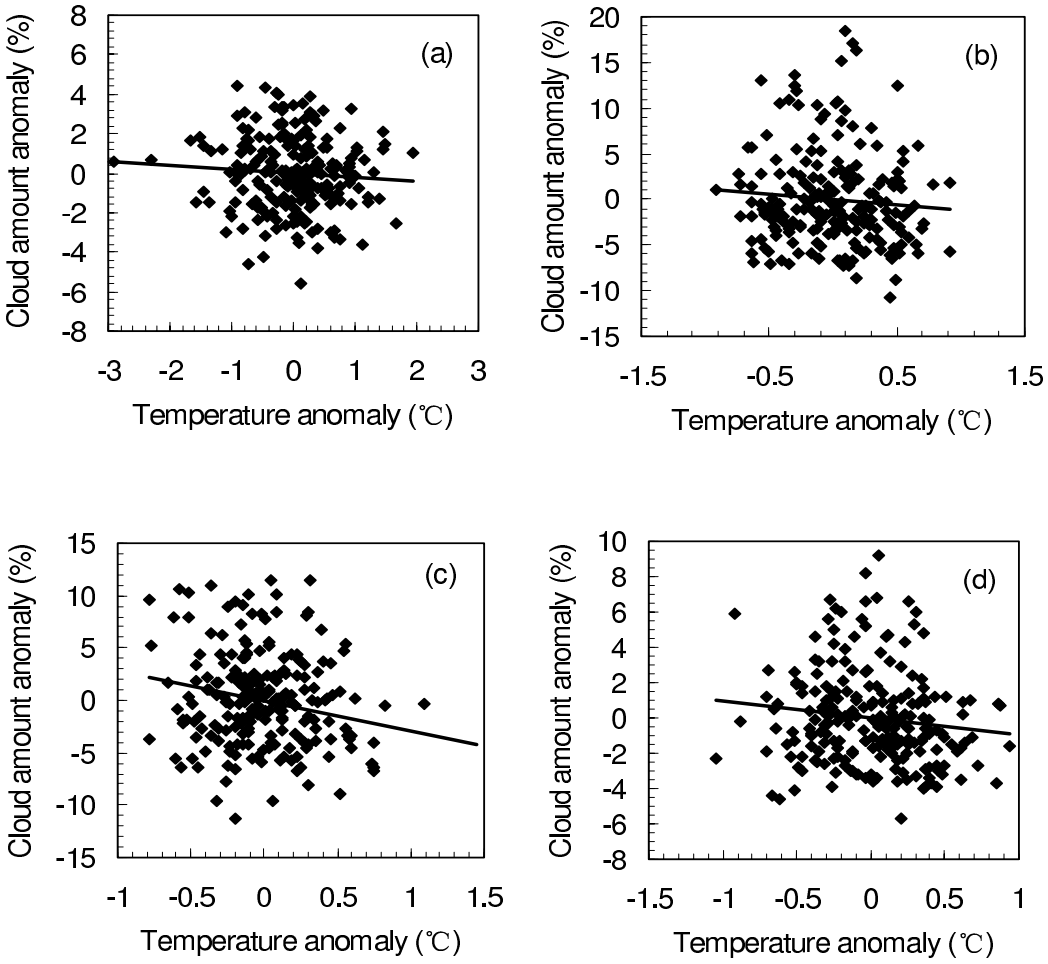

Fig. 9. Scatter plots showing the total cloud amount varies with surface temperature for high latitude (50°–70°N, 60°W–10°E), (b) midlatitude (20–50°N, 60°W–10°E), (c) low latitude (0°–20°N, 60°W–10°E) and (d) total Atlantic ocean region (0°–70°N, 60°W–10°E).

probably causes the climate to become warm conversely.

In order to explore the effect of NAO on the cloud amount, we compare the composite winter (DJFM) cloud anomalies associated with the negative and positive phases of NAO in Fig. 10. The composite years for the negative and positive NAO are listed in Table 4. It is clear that the distribution of cloud amount is sensitive to the phase of the NAO. For the negative phase of NAO, the dominant cloud anomaly field is shown in Fig. 10a. A large zonal band of strong positive anomalies lay across most of the Tropics. The cloud amounts are, however, much less the in mid latitudes. The dominant cloud pattern associated with the positive phase of NAO, shown in Fig. 10b, has a positive anomaly center in the midlatitude storm track region.

Figure 10c shows regions of statistical significance (using the *t*-test with a sample size of 20 points for each grid) for a difference field constructed by subtracting Fig. 10b from Fig. 10a. The significance pattern shows that a positive phase of the Pacific/North America (PNA) pattern is likely to occur with the positive phase of the NAO. This explains why there is a relationship between NAO, cloud and the SST. When the tropical Pacific SST is relatively strong in forcing any particular, distinctive teleconnection pattern will act as a viable linkage or "bridge" between the NAO, cloud and tropical SST anomalies (Huang et al., 1998). Figure 10c also indicates that the anomaly pattern shown in Fig. 10a is less variable (i.e., more stable) than the pattern shown in Fig. 10b.

5. Discussion and conclusions

The NAO is characterized by variations on multiple timescales. We have used a multiresolution Fourier transform (MFT) spectral analysis method to iden-

tify and describe the temporal contributions of various frequency regimes to the overall variability of the NAO. Consistent with some previous studies identified in the paper, a significant portion of the power in the NAO variation comes from three prominent spectral components: (1) annual, (2) interannual, and (3) decadal to interdecadal. The relative contributions of the three components to the total variance of the NAO are not constant in time. Instead, each component itself is strongly modulated on various timescales ranging from interannual to interdecadal. This creates a very complicated MFT spectrum for the NAO, which is characterized by a combined effect of the frequency and amplitude modulations involving bifurication and merging of the dominant frequencies with time.

Our results also show that the blocking formation and cloud amount are strongly related to the phase of the NAO. The blocking pattern mainly reflects the superposition of medium scale waves upon a planetary scale background conducive to block formation as exhibited by the existence of the negative phase of the NAO. The NAO-related differences in blocking frequency and persistence are associated with changes in the zonally-asymmetric thermal forcing. The phase of the NAO, to a large extent, determines the land-sea temperature distribution over the North Atlantic and the adjacent landmass. As elucidated by Charney and DeVore's simplified low-order theoretical model Charney and DeVore, 1979), this distribution in turn controls the nature of the atmospheric flow, which is either an amplified meridional wave-like flow (favourable for block formation), or a more zonally-orientated one, i.e. unfavourable for block formation. Thus a possible physical mechanism that connects blocking episodes to the phases of the NAO is explained in this model. Blocking events in the North Atlantic do also occur during the positive phase of the NAO; however, they are less frequent and their lifetime is considerably shorter than during the negative phase of the NAO.

Although the NAO is the dominant mode of atmospheric variability in the North Atlantic with timescales greater than a month, compared to average lifetimes of approximately 10 days (synoptic timescale) for atmospheric blocks (Knox and Hays, 1985) and hours for clouds, the apparent relationship between the NAO, blocking and cloud in the Atlantic raises some interesting questions, such as: to what extent

Table 4. Years in which the NAO remained in the top tenth percentile (positive) and the bottom tenth percentile (negative) for the December-to-March period. These years are chosen to study the behaviour of cloud amount in the North Atlantic. Years are labelled on January of the averaging period.

Negative NAO	1985	1987	1988	1996	2001
Positive NAO	1989	1990	1992	1993	1995

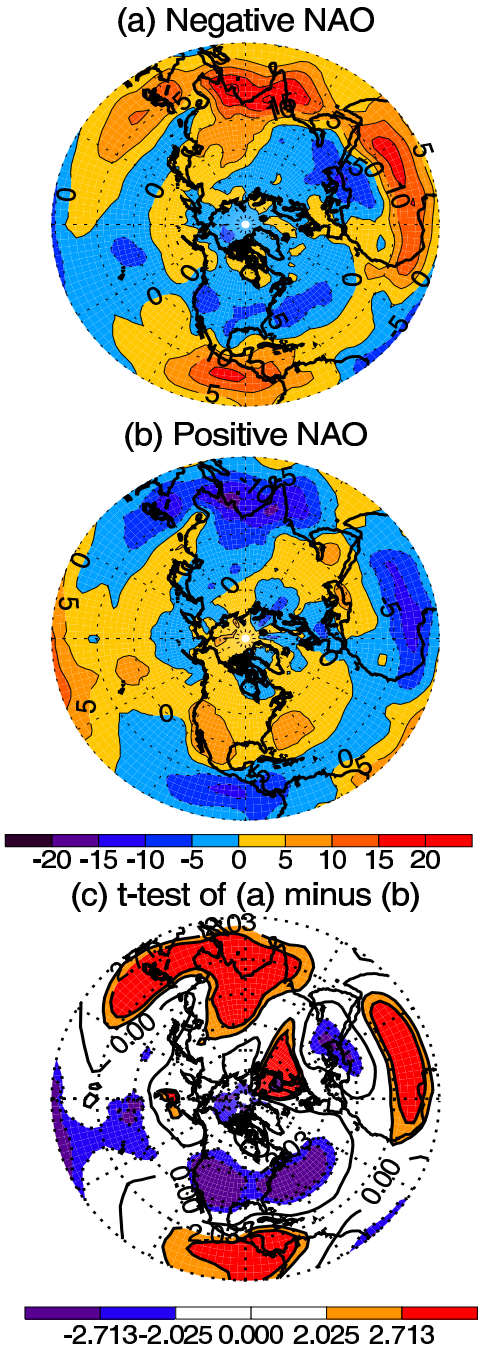

Fig. 10. (a) Composite cloud amount anomaly field of winter (December through March) associated with negative phase of NAO. The contour intervals in percentage are labeled as in the color bar. (b) Same as in (a) but for positive phase of NAO. (c) *t*-test of the (a) minus (b) difference field. Colored areas indicate statistical significance greater than 95% confidence level.

does the low-frequency component of the NAO affect the frequency of blocking and cloud, and what is the dynamical connection between these three phenomena? The linkage between them might be the cloud feedback. Cloud feedback is the coupling that could lead to a change in the clouds, which could then amplify or diminish the initial circulation perturbation. For example, an increase in surface air temperature could increase evaporation, and this in turn might increase the extent of the cloud cover. Increased cloud cover would reduce the radiation reaching the Earth's surface, thereby lowering the surface temperature. The surface temperature then interacts with NAO. This picture of the relationship between NAO, blocking, and cloud is, however, complicated by the temporal and spatial scales involved. More data are required to study such a relationship.

Acknowledgments. This study was supported by the National Natural Sciences Foundation of China under Grant No. 40575036. The ISCCP data were obtained from the NASA Earth Observing System Data and Information System, Distributed Active Center (DAAC) at the Langley Research Center.

REFERENCES

Barnett, T. P., 1985: Variations in near-global sea level pressure. *J. Atmos. Sci.*, **42**, 478–501.

Barnston, A. G., and R. E. Livezey, 1987: Classification, seasonality and persistence of low-frequency atmospheric circulation patterns. *Mon. Wea. Rev.*, **115**, 1083–1126.

Cayan, D. R., 1992: Latent and sensible heat flux anomalies over the northern oceans: The connection to monthly atmospheric circulation. *J. Climate*, **5**, 354–369.

Charney, J., and J. DeVore, 1979: Multiple flow equilibria in the atmosphere and blocking. *J. Atmos. Sci.*, **36**, 1205–1216.

Cook, E. R., R. D. D'Arrigo, and K. R. Briffa, 1998: A reconstruction of the North Atlantic Oscillation using tree-ring chronologies from North America and Europe. *The Holocene*, **8**, 9–17.

Del Genio, A. D., A. A. Lacis, and R. A. Ruedy, 1991: Simulation of the effect of a warmer climate on atmospheric humidity. *Nature*, **351**, 382–385.

Ding, S., G. Shi, and C. Zhao, 2004: Analyzing global trends of different cloud types and their potential impacts on climate by using the ISCCP D2 dataset. *Chinese Science Bulletin*, **49**, 1301–1306.

Dole, R. M., 1989: Life cycles of persistent anomalies. Part I: Evolution of 500 mb height field. *Mon. Wea. Rev.*, **117**, 177–211.

Huang, J., K. Higuchi, and N. B. A. Trivett, 1997: Multiresolution Fourier transform and its application on analysis of CO_2 fluctuations over Alert. *J. Meteor. Soc. Japan*, **75**, 701–715.

Huang, J.-P., K. Higuchi, and A. Shabbar, 1998: The relationship between the North Atlantic Oscillation and El Niño-Southern Oscillation. *Geophys. Res. Lett.*, **25**, 2707–2710.

Hurrell, J. W., 1995: Decadal trends in the North Atlantic Oscillation: Regional temperatures and precipitation. *Science*, **269**, 676–679.

Hurrell, J. W., 1996: Influence of variations in extratropical wintertime teleconnections on Northern Hemisphere temperature. *Geophys. Res. Lett.*, **23**, 665–668.

Hurrell, J. W., and H. van Loon, 1997: Decadal variations in climate associated with the North Atlantic Oscillation. *Climate Change*, **36**, 301–326.

Kalnay, E., and Coauthors, 1996: The NCEP/NCAR 40-year reanalysis project. *Bull. Amer. Meteor. Soc.*, **77**, 437–471.

Knox, J. L., and J. E. Hays, 1985: Blocking signatures in the Northern Hemisphere: Frequency distribution and interpretation. *J. Climatol.*, **5**, 1–16.

Li, J., and Julian X. L. Wang, 2003: A new North Atlantic Oscillation index and its variability. *Adv. Atmos. Sci.*, **20**, 661–671.

Lindzen, R. S., M.-D. Chou, and A. Y. Hou, 2001: Does the earth have an adaptive infrared iris? *Bull. Amer. Meteor. Soc.*, **82**, 417–432.

Nesterov, E. S., 1998: Characteristic features of ocean and atmosphere in different phases of the North Atlantic Oscillation. *Russian Meteorology and Hydrology*, **8**, 58–65.

Rogers, J. C., 1984: The association between the North Atlantic Oscillation and the Southern Oscillation in the Northern Hemisphere. *Mon. Wea. Rev.*, **112**, 1999–2015.

Shabbar, A., J. Huang, K. Higuchi, 2001: The relationship between the wintertime North Atlantic Oscillation and blocking episodes in the North Atlantic. *International Journal of Climate*, **21**(3), 355–369.

Schneider, U., and C.-D. Schonwiese, 1989: Some statistical characteristics of the El Niño/Southern Oscillation and North Atlantic Oscillation indices. *Atmosfera*, **2**, 167–180.

Stockwell, R. G., L. Mansinha, and R. P. Lowe, 1996: Localization of the complex spectrum: The *s* transform. *Journal of the Association of Exploration Geophysicists*, **17**(3), 99–114.

Tibaldi, S., and F. Molteni, 1990: On the operational predictability of blocking. *Tellus*, **42A**, 343–365.

Torrence, C., and G. P. Compo, 1998. A practical guide to wavelet analysis. *Bull. Amer. Meteor. Soc.*, **79**, 61–78.

van Loon, H., and J. C. Rogers, 1978: The seesaw in winter tempertures between Greenland and northern Europe. Part I: General description. *Mon. Wea. Rev.*, **106**, 296–310.

Walker, G. T., and E. W. Bliss, 1932: World weather V. *Mem. Roy. Meteor. Soc.*, **4**, 53–84.

Wilson, R., A. D. Calway, and E. R. S. Pearson, 1992: A generalized wavelet transform for Fourier analysis: The multiresolution Fourier transform and its application to image and audio signal analysis. *IEEE Transaction on Information Theory*, **38**, 674–690.